AMERICAN SOCIETY FOR MICROBIOLOGY | Journal of Virology

Identification and Characterization of a Ribose 2′-*O*-Methyltransferase Encoded by the Ronivirus Branch of *Nidovirales*

Cong Zeng,[a] Andong Wu,[a] Yi Wang,[a] Shan Xu,[a] Yingke Tang,[a] Xu Jin,[a] Shilei Wang,[a] Lei Qin,[a] Ying Sun,[b] Chengpeng Fan,[c] Eric J. Snijder,[d] Benjamin W. Neuman,[e] Yu Chen,[a] Tero Ahola,[f] Deyin Guo[a,c]

State Key Laboratory of Virology, College of Life Sciences, Wuhan University, Wuhan, People's Republic of China[a]; Department of Pathogen Biology, Henan University of TCM, Zhengzhou, Henan, People's Republic of China[b]; Medical Research Institute, School of Basic Medical Sciences, Wuhan University, Wuhan, China[c]; Molecular Virology Laboratory, Department of Medical Microbiology, Leiden University Medical Center, RC Leiden, The Netherlands[d]; School of Biological Sciences, University of Reading, Reading, United Kingdom[e]; Department of Food and Environmental Sciences, University of Helsinki, Helsinki, Finland[f]

ABSTRACT

The order *Nidovirales* currently comprises four virus families: *Arteriviridae*, *Coronaviridae* (divided into the subfamilies *Coronavirinae* and *Torovirinae*), *Roniviridae*, and the recently recognized *Mesoniviridae*. RNA cap formation and methylation have been best studied for coronaviruses, with emphasis on the identification and characterization of two virus-encoded methyltransferases (MTases) involved in RNA capping, a guanine-N7-MTase and a ribose-2′-*O*-MTase. Although bioinformatics analyses suggest that these MTases may also be encoded by other nidoviruses with large genomes, such as toroviruses and roniviruses, no experimental evidence has been reported thus far. In this study, we show that a ronivirus, gill-associated virus (GAV), encodes the 2′-*O*-MTase activity, although we could not detect 2′-*O*-MTase activity for the homologous protein of a torovirus, equine torovirus, which is more closely related to coronaviruses. Like the coronavirus 2′-*O*-MTase, the roniviral 2′-*O*-MTase harbors a catalytic K-D-K-E tetrad that is conserved among 2′-*O*-MTases and can target only the N7-methylated cap structure of adenylate-primed RNA substrates. However, in contrast with the coronavirus protein, roniviral 2′-*O*-MTase does not require a protein cofactor for stimulation of its activity and differs in its preference for several biochemical parameters, such as reaction temperature and pH. Furthermore, the ronivirus 2′-*O*-MTase can be targeted by MTase inhibitors. These results extend our current understanding of nidovirus RNA cap formation and methylation beyond the coronavirus family.

IMPORTANCE

Methylation of the 5′-cap structure of viral RNAs plays important roles in genome replication and evasion of innate recognition of viral RNAs by cellular sensors. It is known that coronavirus nsp14 acts as an N7-(guanine)-methyltransferase (MTase) and nsp16 as a 2′-*O*-MTase, which are involved in the modification of RNA cap structure. However, these enzymatic activities have not been shown for any other nidoviruses beyond coronaviruses in the order *Nidovirales*. In this study, we identified a 2′-*O*-methyltransferase encoded by ronivirus that shows common and unique features in comparison with that of coronaviruses. Ronivirus 2′-*O*-MTase does not need a protein cofactor for MTase activity, whereas coronavirus nsp16 needs the stimulating factor nsp10 for its full activity. The conserved K-D-K-E catalytic tetrad is identified in ronivirus 2′-*O*-MTase. These results extend our understanding of nidovirus RNA capping and methylation beyond coronaviruses and also strengthen the evolutionary and functional links between roniviruses and coronaviruses.

A 5′-terminal cap structure, an N7-methylguanosine linked to the first templated nucleotide via a 5′-5′ triphosphate bridge, is employed widely in viral and eukaryotic cellular mRNAs and plays a critical role in mRNA stability and translation (1–3). The basic cap-0 structure m7GpppN is formed by sequential reactions catalyzed by an RNA triphosphatase, a guanylyltransferase, and a guanine-N7-methyltransferase (N7-MTase) (1, 2, 4). In higher eukaryotes and most viruses, the cap-0 structure is further methylated at the ribose 2′-O position of the first nucleotide by ribose 2′-*O*-methyltransferase (2′-*O*-MTase) to form a cap-1 structure (m7GpppNm2) (4–6). Recently, it has been reported that 2′-O methylation of the cap of viral mRNAs is important for RNA viruses to evade host innate immune responses by preventing the recognition of their mRNAs as "nonself" (7, 8). Therefore, viral 2′-MTase represents a potential target for antiviral drug development. Generation of 2′-*O*-MTase-deficient viruses has been used as a strategy to develop effective live attenuated vaccines (9–12). Chemical and polypeptide inhibitors targeting viral 2′-*O*-MTase have been shown to function as antivirals (13–15).

The order *Nidovirales* includes the most complex positive-sense single-stranded RNA (ssRNA) viruses with human and animal hosts, including the highly pathogenic severe acute respiratory syndrome coronavirus (SARS-CoV) and Middle East respiratory syndrome coronavirus (MERS-CoV). It currently consists of four virus families, *Arteriviridae* (12.7- to 15.7-kb genomes; known as small-genome nidoviruses), *Coronaviridae*, *Roniviridae*, and the recently recognized *Mesoniviridae* (26.3 to

Received 7 April 2016 **Accepted** 4 May 2016

Accepted manuscript posted online 11 May 2016

Citation Zeng C, Wu A, Wang Y, Xu S, Tang Y, Jin X, Wang S, Qin L, Sun Y, Fan C, Snijder EJ, Neuman BW, Chen Y, Ahola T, Guo D. 2016. Identification and characterization of a ribose 2′-*O*-methyltransferase encoded by the ronivirus branch of *Nidovirales*. J Virol 90:6675–6685. doi:10.1128/JVI.00658-16.

Editor: S. Perlman, University of Iowa

Address correspondence to Deyin Guo, dguo@whu.edu.cn.

31.7 kb) (the last three families are referred to as large-genome nidoviruses) (16). The family *Coronaviridae* is further divided into two subfamilies, *Coronavirinae* (for coronaviruses) and *Torovirinae* (for toroviruses). Nidovirus replicative enzymes are evolutionarily related, and the viruses share several common features, like the synthesis of a set of subgenomic mRNAs from subgenome-length negative-stranded templates and the acquisition of various RNA-processing enzymes that play roles in virus replication (17). In the past decade, cap formation and methylation in coronaviruses have been extensively studied, focusing on two virus-encoded *S*-adenosyl-L-methionine (SAM, or AdoMet)-dependent MTases: an N7-MTase and a 2′-*O*-MTase. Our previous work has demonstrated that one of the functions of coronavirus nonstructural protein 14 (nsp14) is to act as an N7-MTase (18, 19), while other studies have shown that coronavirus nsp16 acts as a 2′-*O*-MTase (20). In the case of SARS-CoV, that role requires the viral cofactor nsp10, although feline coronavirus (FCoV) nsp16 also displayed activity in the absence of nsp10 (5, 15, 20–22). However, there is no experimental evidence to show that any other nidoviruses (except coronaviruses) possess a functional methyltransferase.

Gill-associated virus (GAV) is the type species of the genus *Okavirus* in the family *Roniviridae* of the order *Nidovirales* and has been associated with mortalities in black tiger shrimps (*Penaeus monodon*) and economic losses to shrimp farming in eastern Australia (23, 24). GAV (genotype 2) is one of six known genotypes in the yellow head complex of nidoviruses, which also contains yellow head virus (YHV) (genotype 1) and four other genotypes (25). GAV and YHV are morphologically indistinguishable, and they are both highly pathogenic for *P. monodon* (26, 27). GAV, as well as the other five genotypes, is an enveloped, rod-shaped, positive-sense ssRNA virus with a genome of about 26 kb (23, 25, 28). In common with other nidoviruses, the 5′-terminal 20 kb of the GAV genome includes two long, overlapping open reading frames (ORFs) and is translated into two large polyproteins, pp1a and pp1ab, via a −1 ribosomal frameshift (29). ORF1a encodes a putative papain-like protease and a putative 3C-like protease that bridge the gap between the distantly related chymotrypsin-like cysteine proteinases of coronaviruses and potyviruses (30, 31). It was predicted that pp1ab contains a putative helicase (HEL) domain, RNA-dependent RNA polymerase (RdRp) synthesis, an exonuclease (Exon) domain, and an MTase domain in an order similar to that of other nidoviruses (17, 29), suggesting that GAV shares a common ancestor with the other members of the nidoviruses. GAV and the closely related YHV appear to be the first nidoviruses isolated from an invertebrate, and as marine invertebrates are prior to vertebrates in evolution, GAV may be a relic of the ancient nidovirus (29). The newly identified alphamesonivirus 1, which belongs to the *Mesoniviridae* and also infects invertebrate hosts, has phylogenetic relationship to the *Coronaviridae*, and phylogenetic analysis has shown that nidoviruses may have evolved from arthropods (32, 33).

According to bioinformatics analysis, all nidoviruses except arteriviruses encode a 2′-*O*-MTase domain at the C-terminal end of their large pp1ab replicase polyprotein, whereas all large-genome nidoviruses except toroviruses possess an N7-MTase domain following their exoribonuclease domain (17, 32, 34). We have attempted to address whether the large-genome noncoronaviral nidoviruses also encode methyltransferases involved in viral RNA cap methylation by utilizing the genetic and biochemical methodologies established in our laboratory (5, 18), but we failed to detect N7-MTase activity for any of the proteins encoded by roniviruses, mesoniviruses, and toroviruses (unpublished results). In this study, we show that the MTase domain of a ronivirus (GAV) (arbitrarily named "nsp16" by analogy with the location and function of its coronavirus homolog), but not the corresponding torovirus domain (also named nsp16), possesses 2′-*O*-MTase activity *in vitro*. We further demonstrate that ronivirus nsp16 alone can efficiently execute its MTase activity, which is in contrast with coronavirus nsp16, which requires virus-encoded nsp10 as a cofactor for its full function (15). These results extend our understanding of nidovirus RNA capping and methylation and strengthen the evolutionary and functional links between roniviruses and coronaviruses.

MATERIALS AND METHODS

Radioactive reagents. *S*-Adenosyl[methyl-^{3}H]methionine (67.3 Ci/mmol; 0.5 μCi/μl) and [α-^{32}P]GTP (3,000 Ci/mmol; 10 mCi/ml) were purchased from PerkinElmer.

Cloning, expression, and protein purification. The genomic cDNA of shrimp GAV, the type species of the *Roniviridae*, was kindly provided by J. A. Cowley and was used as the template to construct the expression constructs. Two pairs of PCR primers were used to amplify the gene fragments of GAV: 5′-CGGGATCCCTCAGTTACTCAGGCACCGC-3′ (sense) and 5′-CCCTCGAGCTCGTGCTTGACTGGGATGG-3′ (antisense) for GAV nsp10 and 5′-CGGGATCCCTCTACCACGTCGCTCCTAC-3′ (sense) and 5′-CCCTCGAGAAATTTGATGAATCTGGGAG-3′ (antisense) for GAV nsp16, which correspond to nucleotides 11703 to 12212 and 19403 to 20089 of the GAV genome (GI|166851932), respectively. These PCR products were cloned into the *Escherichia coli* expression vector pGEX-6p-1, resulting in the expression constructs pGEX-6p-1-GAV nsp10 and pGEX-6p-1-GAV nsp16. The mutant plasmids of GAV nsp16 were generated by one-step PCR with mutagenic primers.

E. coli BL21(DE3), transformed with pGEX-6p-1-GAV nsp10 or nsp16, was grown in Luria broth (LB) medium containing ampicillin at 37°C. When the optical density at 600 nm (OD_{600}) of the culture reached 0.6, isopropyl-β-D-thiogalactopyranoside (IPTG) was added to a final concentration of 0.4 mM and induced at 16°C for 16 h. Bacterial cells were harvested by centrifugation and lysed by sonication. Glutathione *S*-transferase (GST)-tagged fusion proteins were purified from the cell lysate by affinity chromatography using glutathione resin (GenScript) according to the manufacturer's instructions. GAV nsp10 (pp1a residues 3879 to 4048; 170 amino acids [aa]) fused with an N-terminal GST tag is about 45 kDa, which was confirmed by SDS-PAGE. GAV nsp16 (pp1ab residues 6446 to 6673; 228 aa) carrying an N-terminal GST tag was about 52 kDa.

The genes of equine torovirus (EToV) were obtained by PCRs with the template of EToV genome cDNA (GI|190360102), kindly provided by Eric J. Snijder. We performed bioinformatics analysis to predict the proteinase cleavage sites and arbitrarily named the most C-terminal cleavage product of pp1b EToV nsp16 (the predicted 2′-MTase domain) and named the putative cleavage product that is upstream of the 2′,5′-phosphodiesterase domain of pp1a EToV nsp10. The following primers were used to amplify the gene fragments: sense, 5′-CGGGATCCGGTGTTAGATTGGGAGGTGT-3′, and antisense, 5′-CCCTCGAGCTGAGGCTTAAAAACTGGA-3′ for EToV nsp10 (nucleotides [nt] 13560 to 14018 of the genome) and 5′-CGGGATCCAAGGATTTTGTAAGGTCGTA-3′ (sense) and 5′-CCCTCGAGATGTTCCATTTGGCACAAC-3′ (antisense) for EToV nsp16 (nt 20597 to 21391). The PCR fragments were cloned into *E. coli* expression vectors pET30a and pGEX-6p-1, respectively, generating the plasmids pET30a-EToV nsp10 and pGEX-6p-1-EToV nsp16.

The GST fusion protein EToV nsp16 (pp1ab residues 6593 to 6857; 265 aa) was expressed and purified similarly to GAV nsp16, and the fusion protein size was 57 kDa. pET30a-EToV nsp10 was transformed into *E. coli*

BL21(DE3), and the cells were grown in LB medium containing kanamycin at 37°C. When the OD_{600} of the culture reached 0.6, IPTG was added to a final concentration of 0.4 mM, and the culture was grown for an additional 16 h at 16°C. The bacterial cells were harvested by centrifugation and lysed by sonication. The C-terminally 6-histidine-tagged protein EToV nsp10 was purified from the cell lysate by affinity chromatography using Ni-nitrilotriacetic acid (NTA) according to the manufacturer's instructions (Qiagen). EToV nsp10 (pp1a residues 4247 to 4399; 153 aa) was 17 kDa in size. The predicted sizes of these two proteins were in accordance with their sizes in SDS-PAGE analysis.

SARS-CoV nsp10 and nsp16 were expressed and purified as described in our previous work (5).

Preparation of RNA substrates. An RNA corresponding to the 68-nt 5′-untranslated region (UTR) of GAV was transcribed *in vitro* using the PCR products as a template, and the template was amplified from GAV cDNA (the primers were as follows: 5′-CAGTAATACGACTCACTATTA CGTTACGTTCCACGTAC-3′ and 5′-GGTCGGAAACGCTGGAAAAC-3′). Since the first nucleotide of the GAV genome is an adenine, we used a bacteriophage T7 ϕ2.5 promoter to direct the synthesis of an RNA transcript starting with an adenine. A MEGAscript kit (Life Technologies) was used to transcribe RNA *in vitro* with 100 ng of PCR template in a 20-μl reaction volume. The reaction mixture was mixed thoroughly and incubated for 16 h at 37°C. After the reaction, 2 units of Turbo DNase was added, followed by a further incubation for 15 min at 37°C. For purification of RNA, the transcription reaction mixture was extracted with phenol-chloroform-isoamyl alcohol, precipitated with 75% ethanol containing sodium acetate, resuspended in RNA-free water (TianGen), and quantitated with a Nanodrop 2000c (Thermo Scientific). The nonviral RNA substrates $pppAC_n$, $pppUC_{20}$, $pppGC_{20}$, and $pppCC_{20}$ were transcribed and purified as described previously (5).

Capped RNAs (GpppRNA and ^{7Me}GpppRNA) were produced using the Vaccinia Capping System (New England BioLabs), purified through Sephadex G-25 quick-spin columns (Roche), extracted with phenol-chloroform-isoamyl alcohol, and precipitated with ethanol. ^{32}P-labeled RNA substrates (G*pppRNA and ^{7Me}G*pppRNA; the asterisks indicate that the phosphates that follow were ^{32}P labeled) used for thin-layer chromatography (TLC) were synthesized as described previously (18).

Biochemical assay for methyltransferase activity. The ^{32}P-labeled 2′-*O*-MTase assay was performed in an 8.5-μl reaction system (containing 50 mM Tris-HCl [pH 8.0], 2 mM dithiothreitol [DTT], 2 mM $MgCl_2$, 10 units RNase inhibitor, 2×10^3 cpm of ^{7Me}G*pppA-RNA, 0.2 mM SAM, and 0.5 μg of purified proteins or mutant proteins) at 20°C for 1 h. The control substrates G*pppA-RNA and ^{7Me}G*pppA-RNA were prepared using the vaccinia virus protein D1-D12, which has the activities of both GTase and N7-MTase, by incubating them at 37°C for 1 h and were purified as described previously (5). Control ^{7Me}G*pppAm-RNA was produced by incubation of ^{7Me}G*pppA-RNA with the vaccinia virus 2′-*O*-methyltransferase VP39 (Epicentre) at 37°C. The radiolabeled capped RNAs were digested with nuclease P1 (U.S. Biological) to release the cap structures and were then loaded onto polyethyleneimine cellulose F plates (Merck) for TLC analysis and developed in 0.65 M LiCl. The formation of the ^{32}P-labeled cap structure was determined by scanning the chromatogram with a phosphorimager as described previously (5, 18).

The ^{3}H-methyl incorporation MTase activity assays were performed in a 20-μl reaction system (containing 50 mM Tris-HCl [pH 8.0], 2 mM DTT, 2 mM $MgCl_2$, 40 units of RNase inhibitor, 0.01 mM SAM, 0.5 μCi of *S*-adenosyl[methyl-3H]methionine [67.3 Ci/mmol; 0.5 μCi/μl], 1 μg proteins, and 3 μg of ^{7Me}GpppRNA substrates) at 37°C for 1 h. The ^{3}H-labeled products were isolated using DEAE-Sephadex A-50 columns and quantitated by liquid scintillation counting (PerkinElmer) as described previously (5, 35).

Multiple-sequence alignment and homology modeling. The alignment of the nsp16 protein sequences from different *Nidovirales* species was performed by using ClustalX, and the result was imported into ESPript 3.0, together with the three-dimensional (3D) structure of SARS-CoV nsp16/nsp10 (Protein Data Bank [PDB] accession no. 3R24) to assign the secondary structure. The predicted 3D structure of GAV nsp16 was generated using the SARS-CoV nsp16 template (PDB 3R24, chain A). The multiple-sequence alignment was done with ClustalX and then uploaded to SWISS-MODEL for structural modeling, which was further analyzed by PyMol.

RESULTS

Ronivirus nsp16 possesses SAM-dependent 2′-*O*-MTase activity in the absence of another protein cofactor. Bioinformatics analysis revealed that all large nidoviruses encode a putative 2′-*O*-MTase domain located at the most C-terminal end of the replicase pp1ab polyprotein (17). As coronaviral nsp16, with nsp10 as a cofactor for full activity, has been demonstrated to be a functional 2′-*O*-MTase (5, 15, 21, 22), we further tested the homologous proteins of toroviruses and roniviruses for 2′-*O*-MTase activity. For this purpose, we selected two representative viruses, EToV (36), which belongs to the subfamily *Torovirinae* of the *Coronaviridae* and is more closely related to coronaviruses, and GAV (24, 29), which belongs to the *Roniviridae* and is much more distantly related to coronaviruses. As the proteinase cleavage sites are not completely established for the large polyprotein 1ab of these two viruses (30, 36), their protein counterparts for coronavirus nsp16 and nsp10 are arbitrarily named EToV or GAV nsp16 and nsp10, respectively, in analogy to CoV protein nomenclature. The well-characterized 2′-*O*-MTases SARS-CoV nsp10/nsp16 and vaccinia virus VP39 were used as controls (5, 15). The locations of the predicted proteinase cleavage sites and the nsp10 and nsp16 homologs in the pp1ab polyprotein of EToV and GAV are indicated in Fig. 1A. It is notable that FCoV nsp16 can exert low activity of 2′-*O*-MTase in the absence of nsp10 (20); however, our group has conducted an extensive analysis of the stimulating activities of nsp10 proteins of different coronaviruses, and we showed that the MTase activity of FCoV nsp16 can also be markedly enhanced in the presence of nsp10 (15), indicating that the stimulating activity of nsp10 is universal to all the coronaviruses, including FCoV.

As shown in Fig. 1B, recombinant nsp10 and nsp16 of EToV, GAV, and SARS-CoV could be abundantly expressed in *E. coli* cells and purified to more than 95% homogeneity by affinity chromatography.

To test the predicted 2′-*O*-MTase activities of these viral proteins, we first conducted 2′-*O*-MTase activity assays *in vitro* using a 21-nt RNA substrate (the cap-0 ^{7Me}GpppAC$_{20}$) that was capped and methylated at the N7 position of the cap. Transfer of the ^{3}H-labeled methyl group from SAM to cap-0 RNA substrates should result in cap-1 RNA (^{7Me}GpppAmC$_{20}$), which can be measured quantitatively by liquid scintillation detection. As the natural hosts of GAV are shrimps (*P. monodon*), which naturally have a lower body temperature than mammals, all assays with GAV proteins were performed at 20°C while all the other assays were at 37°C. As shown in Fig. 1C, GAV nsp16, in either the presence or absence of GAV nsp10, showed remarkable 2′-*O*-MTase activity, similar to that of vaccinia virus VP39 and SARS-CoV nsp10/nsp16, whereas EToV nsp16 alone or in combination with nsp10 did not display any 2′-*O*-MTase activity, similar to the negative control (SARS-CoV nsp10 alone). These results indicate that GAV nsp16 alone possesses 2′-*O*-MTase activity, which is different from coronavirus nsp16, which requires nsp10 as a stimulating cofactor.

We further tested the 2′-*O*-MTase activity of GAV nsp16 with

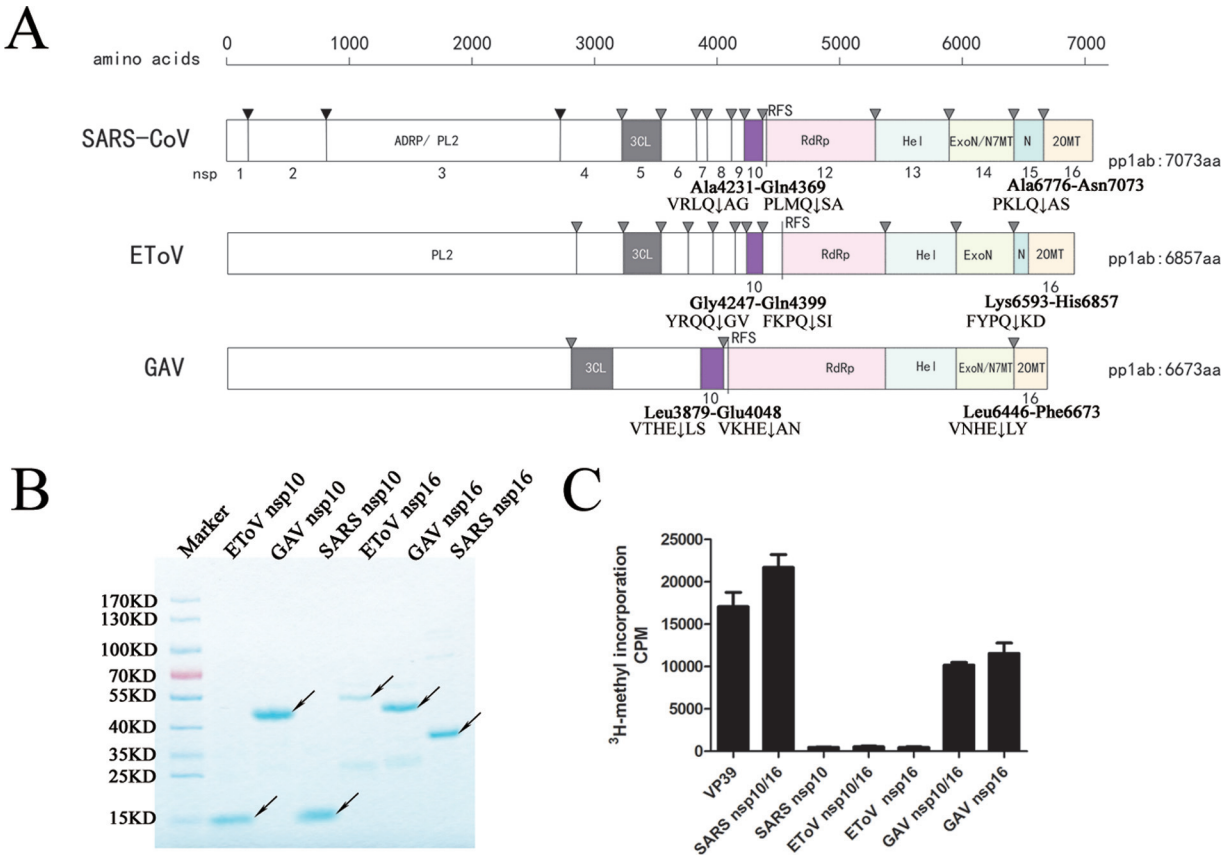

FIG 1 Identification of nidovirus 2′-*O*-MTases. (A) Domain organization of the replicase pp1ab polyprotein for selected nidoviruses: SARS-CoV (coronavirus), EToV (torovirus), and GAV (ronivirus). The predicted domains are indicated, and the predicted cleavage sites are marked with arrowheads. The domains are as follows: ADP-ribose-1′-phosphatase (ADRP), papain-like proteinases (PLpro), chymotrypsin-like proteinase (3CLpro), RNA-dependent RNA polymerase (RdRp), helicase (Hel), exonuclease (ExoN), N7-methyltransferase (N7MT), uridylate-specific endoribonuclease (Ne; also abbreviated NendoU), and 2′-*O*-methyltransferase (2OMT). The coronavirus nsp10 and its similarly located counterparts in EToV and GAV are depicted in purple, and RFS stands for the ribosomal frameshift site. The start sites and endpoints of the expressed proteins are indicated. (B) Expression and purification of recombinant viral proteins. The gels of SDS-PAGE were stained with Coomassie brilliant blue. GAV nsp10, GAV nsp16, and EToV nsp16 are GST fusion proteins, and the others were 6-histidine tagged. These protein bands are indicated with black arrows. (C) Activities of potential 2′-*O*-methyltransferases in ^{3}H-methyl incorporation assays. Vaccinia virus VP39 and SARS-CoV nsp10/nsp16 were used as positive controls, while SARS-CoV nsp10 acted as a negative control for 2′-*O*-MTase activity. The final concentration of the nsp16 proteins of SARS-CoV, GAV, and EToV was 1 μM. The cpm values reflect the 2′-*O*-MTase activity that was detected by liquid scintillation counting. The error bars indicate standard deviations.

capped RNA substrates representing the 5′-terminal 68 nt of the viral genome (^{7Me}G*pppA-RNA, where the asterisk indicates that the phosphate that follows was ^{32}P labeled). GAV nsp16 was incubated with ^{7Me}G*pppA-RNA in the presence of 0.2 mM SAM. After incubation, the RNA was digested with nuclease P1 to release the cap structure and analyzed on TLC plates (Fig. 2A, lane 1). The radiolabeled cap analogs G*pppA, ^{7Me}G*pppA, and ^{7Me}G*pppAm, generated by vaccinia virus D1/D12 and VP39, were used as controls (Fig. 2A, lanes 2, 3, and 4). When the 2′-O position of the first nucleotide of the substrates was methylated, the released cap structure was ^{7Me}G*pppA$_m$, and the 2′-O-methylated and unmethylated cap structures could be readily separated on TLC plates. As shown in Fig. 2A, the 2′-O-methylated cap (^{7Me}G*pppA$_m$) (Fig. 2A, lane 4) generated by VP39 migrated more slowly than a cap-0 structure lacking 2′-O methylation (^{7Me}G*pppA) (Fig. 2A, lane 3), which was used as a reference for the reaction products of GAV nsp16. The migration of the cap structure released from ^{7Me}G*pppA-RNA treated with GAV nsp16 corresponded to that of ^{7Me}G*pppAm, further confirming that GAV nsp16 functions as a methyltransferase that adds a methyl group in the ribose 2′-O position.

GAV nsp16 specifically methylates the N7-methylated cap-0 structure of RNA substrates with a 5′-terminal A. Next, we explored whether GAV nsp16 could methylate capped RNA GpppAC$_n$ that was not methylated at the N7 position. As shown in Fig. 2B, when the uncapped RNA oligonucleotide pppAC$_{20}$ and the capped RNA oligonucleotide GpppAC$_{20}$ (which is not methylated at the N7 position) were used as substrates, ^{3}H-methyl groups could not be incorporated either by GAV nsp16 or by SARS-CoV nsp16/nsp10. In contrast, when RNA oligonucleotides containing an N7-methylated cap-0 structure, ^{7Me}GpppAC$_{20}$ (black bars in Fig. 2B), were used as substrates, efficient incorporation of ^{3}H-methyl groups by both GAV nsp16 and SARS-CoV nsp16/nsp10 was observed. These data suggest that GAV nsp16 can methylate only the cap-0 structure of RNA substrates (^{7Me}GpppA-RNA), similarly to the coronavirus 2′-*O*-MTase.

It had been reported that vaccinia virus VP39 is a 2′-*O*-MTase that modifies 5′-capped mRNA without any sequence specificity

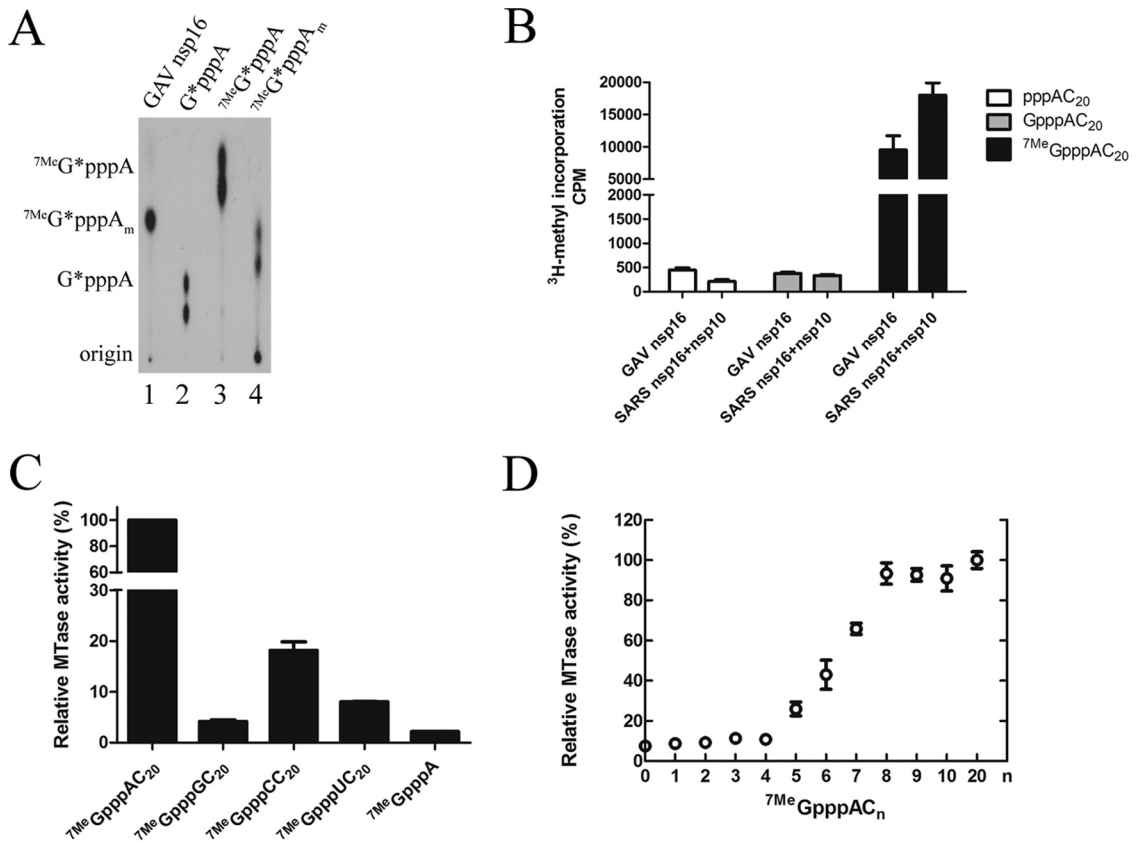

FIG 2 RNA substrate specificity of GAV nsp16 2′-*O*-MTase. (A) (Lane 1) An RNA representing the first 68 nucleotides of the GAV genome was capped to form ^{7Me}G*pppA-RNA, incubated with GAV nsp16, digested by nuclease P1 to release cap structures, and analyzed by TLC. (Lanes 2 to 4) Cap analogs used as controls were generated by vaccinia virus capping enzymes D1/D12 in the absence of SAM (lane 2), in the presence of SAM (lane 3), and with SAM and VP39 2′-*O*-MTase (lane 4). (B) SAM-dependent methyltransferase activities of GAV nsp16 and SARS nsp16. Equal amounts of proteins were incubated with AC_{20} (white), $GpppAC_{20}$ (gray), and $^{7Me}GpppAC_{20}$ (black) in the presence of ^{3}H-labeled SAM for 1 h, and radioactivity incorporation was detected by liquid scintillation counting. (C) MTase activities of GAV nsp16 for capped RNAs with different initiating nucleotides. $^{7Me}GpppAC_{20}$, $^{7Me}GpppCC_{20}$, $^{7Me}GpppUC_{20}$, $^{7Me}GpppGC_{20}$, and $^{7Me}GpppA$ were used as substrates to test GAV nsp16 activity. (D) GAV nsp16 2′-*O*-MTase activities on capped RNA substrates of different lengths. The activity was formulated as a percentage (100% corresponds to the activity of $^{7Me}GpppAC_{20}$). The error bars indicate standard deviations.

(37). However, in our previous study, we found that SARS-CoV nsp16 MTase methylated ^{7Me}GpppA-RNA, but not ^{7Me}GpppG-RNA (5), indicating that SARS-CoV nsp16 is a sequence-dependent 2′-*O*-methyltransferase acting on substrates starting with A. In a similar way, we studied the substrate specificity of GAV nsp16. A variety of capped RNA oligonucleotides (initiated with different nucleotides followed by 20 cytidines, $^{7Me}GpppAC_{20}$, $^{7Me}GpppCC_{20}$, $^{7Me}GpppUC_{20}$, and $^{7Me}GpppGC_{20}$) and the cap analog (^{7Me}GpppA) were treated with purified GAV nsp16 in the presence of ^{3}H-labeled SAM, after which the products were purified and measured by liquid scintillation counting. As shown in Fig. 2C, GAV nsp16 had robust activity on the substrate $^{7Me}GpppAC_{20}$ but no detectable activity on $^{7Me}GpppUC_{20}$ and $^{7Me}GpppGC_{20}$ (Fig. 2C). Of note, GAV nsp16 showed marginal activity on the substrate $^{7Me}GpppCC_{20}$. These results indicate that GAV nsp16 2′-*O*-MTase has a strong preference for ^{7Me}GpppA-initiated RNA, similar to SARS-CoV nsp10/nsp16. Consistent with our observation, the very 5′-terminal nucleotide of roniviruses is a conserved adenylate in all the genome sequences that have been sequenced.

There was no activity of GAV nsp16 when the cap analog ^{7Me}GpppA was used as the substrate (Fig. 2C), suggesting that the length of the RNA substrate is relevant for GAV nsp16 2′-*O*-MTase activity *in vitro*. We next investigated the correlation between MTase activity and RNA substrate length. RNA substrates of different lengths ($^{7Me}GpppAC_n$, where n ranges from 0 to 20) were obtained as described in Materials and Methods and treated with equal amounts of purified GAV nsp16. As shown in Fig. 2D, there was no detectable 2′-*O*-MTase activity on RNA substrates shorter than 5 nucleotides. There was marginal activity when the RNA length reached 6 nucleotides ($n = 5$), and the activity increased gradually with the increase of RNA substrate length ($n = 5$ to 8). The activity of GAV nsp16 reached a plateau when the RNA length exceeded 9 nucleotides ($n > 8$). These results imply that the *in vitro* 2′-*O*-MTase activity of GAV nsp16 requires a certain length of RNA substrate for full activity.

Biochemical parameters of GAV nsp16 activity. As the natural hosts for roniviruses are invertebrates, we further characterized the biochemical parameters and optimal reaction conditions for GAV nsp16 *in vitro*. First, the optimal temperature of the GAV nsp16 methyltransferase reaction was determined. Since shrimps, which are the natural hosts of GAV, live in environments with low or variable temperatures, a temperature range from 10°C to 37°C was tested. As shown in Fig. 3A, a typical bell-shaped distribution

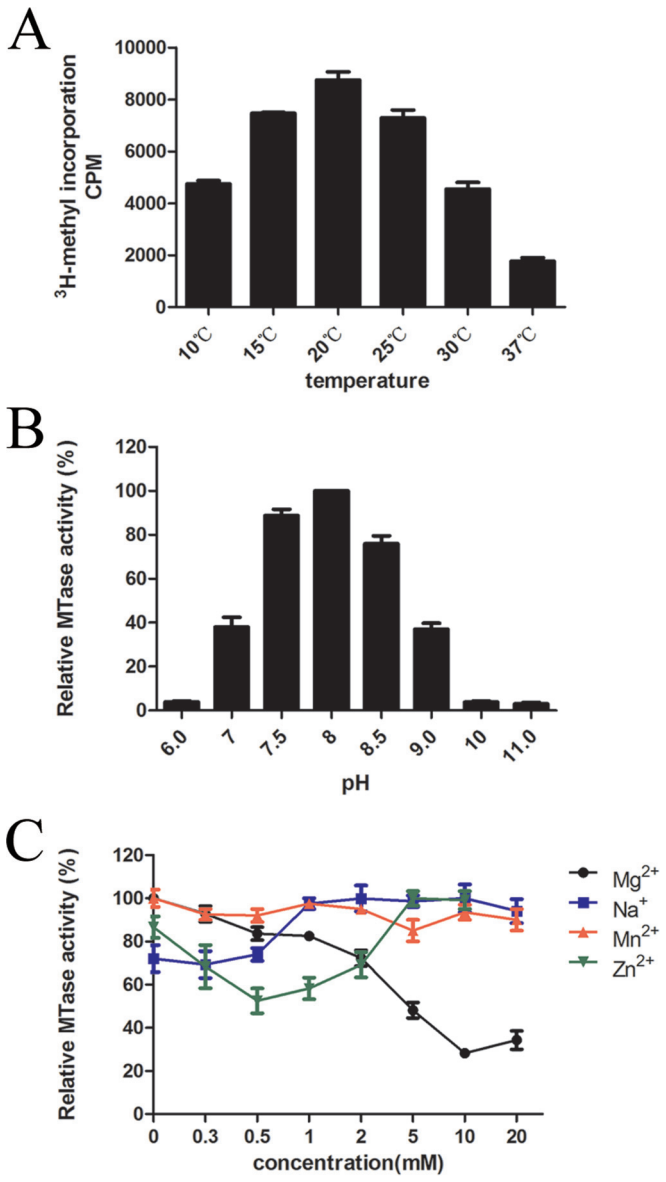

FIG 3 Determining the optimal reaction conditions for GAV nsp16. The GAV nsp16 activity was measured in the presence of ^{3}H-labeled SAM by liquid scintillation counting of transferred ^{3}H-methyl. (A) Effect of temperature on enzymatic activity. Reactions were performed in Tris buffer (pH 8.0) with incubation at various temperatures. RNAs were purified with Sephadex A-50 and detected by liquid scintillation counting. (B) Enzymatic activities of GAV nsp16 at different pH values, including citric acid-NaOH (pH 6.0), Tris-HCl buffer (pH 7.0 to 9.0), and Na_2CO_3-NaOH buffer (pH 10 and 11). An activity of 100% corresponds to that at pH 8.0. (C) Influence of positive-valence metal ions on enzymatic activity. The reactions were conducted at pH 8.0 and 20°C. The error bars indicate standard deviations.

was obtained, with optimal activity at 20°C, indicating that the GAV enzyme is more active at a temperature that corresponds to the natural ambient temperature of its host. In contrast, the 2′-*O*-MTases of coronaviruses that infect mammalian hosts adopt a higher temperature for optimal enzymatic activity (5).

We next tested the influence of pH on GAV nsp16 activity. pH values between 6.0 and 11.0 were used, and this activity profile also fit a bell-shaped distribution similar to that obtained when testing the influence of the reaction temperature (Fig. 3B). The GAV 2′-*O*-MTase had optimal activity at pH 8.0.

We also investigated the effect of divalent ions on GAV nsp16 at the optimal temperature and pH, since it has been reported that divalent ions can stimulate the methyltransferase activities of several 2′-*O*-MTases (20, 38). Mn^{2+}, Mg^{2+}, and Zn^{2+} were tested in our assay. Surprisingly, none of these divalent ions could stimulate the activity of GAV nsp16. On the contrary, higher concentrations of Mg^{2+} even markedly suppressed the activity of GAV nsp16 (Fig. 3C). We also determined the influence of Na^+ on GAV nsp16, as some 2′-*O*-MTases can tolerate only very low Na^+ concentrations (39). Interestingly, GAV nsp16 was not inhibited by a concentration of Na^+ as high as 20 mM, which is different from dengue virus $NS5MTase_{DV}$ 2′-*O*-MTase (39) and vaccinia virus VP39 (40).

The conserved K-D-K-E catalytic tetrad of the GAV 2′-*O*-MTase is required for activity. The group of 2′-*O*-methyltransferases contains a conserved K-D-K-E catalytic tetrad, which is vital for RNA 2′-*O*-MTase activity (20, 41, 42). To identify the K-D-K-E catalytic tetrad of GAV nsp16, we made a comparative analysis of GAV nsp16 with coronavirus nsp16. The multiple-sequence alignment is shown in Fig. 4A. For SARS-CoV, the conserved K-D-K-E residues of nsp16 were first predicted (Lys-46, Asp-130, Lys-170, and Glu-203) and were subsequently confirmed by crystal structure analysis (5, 22). The amino acids marked with asterisks in Fig. 4A constitute the predicted K-D-K-E tetrad of GAV nsp16 (Lys-39, Asp-114, Lys-144, and Glu-178), which are completely conserved in the 2′-*O*-methyltransferases of nidoviruses. We next generated a structural model of GAV nsp16 (Fig. 4B) by homology-based modeling, using SARS-CoV nsp16 as the template (Fig. 4C). As shown in the schematic diagrams of their structural topologies (Fig. 4D), GAV nsp16 and SARS-CoV nsp16 share similar global structures, with a parallel array of β-strands surrounded by a number of α-helices and loops. The residues of the predicted K-D-K-E tetrad in GAV nsp16 are located in an α-helix with three parallel β-strands, whose positions are similar to those in SARS-CoV nsp16. However, the structural model predicts that GAV nsp16 possesses a six-stranded β-sheet instead of the seven-stranded β-sheet of many known 2′-*O*-methyltransferases (5, 43). The missing β-strand of GAV nsp16 would correspond to β-strand 3 (β3) of SARS-CoV nsp16 (Fig. 4A and D), but clearly, this structural difference first needs to be confirmed by future direct analysis of the structure of GAV nsp16.

To experimentally confirm the importance of the K-D-K-E catalytic tetrad of GAV nsp16, the four residues (K39, D114, K144, and E178) were mutated to either alanine or an amino acid residue with similar chemical properties (R for K, E for D, and D for E). In ^{3}H-methyl incorporation MTase activity assays, we found that the wild-type enzyme possessed about 50% of the activity of SARS-CoV nsp10/nsp16 (the positive control) when tested under their respective optimal conditions (Fig. 5A and B). When any of the four GAV residues was mutated to alanine, the 2′-*O*-MTase activity was completely abolished (Fig. 5A and B). When more conservative substitutions were made, GAV nsp16 2′-*O*-MTase activity was largely disrupted, but a trace amount of activity could be observed (Fig. 5A and B). This indicates that both the charges and the steric properties of the tetrad residues of GAV nsp16 influence its MTase activity. For these assays, two RNA substrates, the capped 5′-terminal 68 nt of the GAV genome (^{7Me}Gppp-5′ UTR)

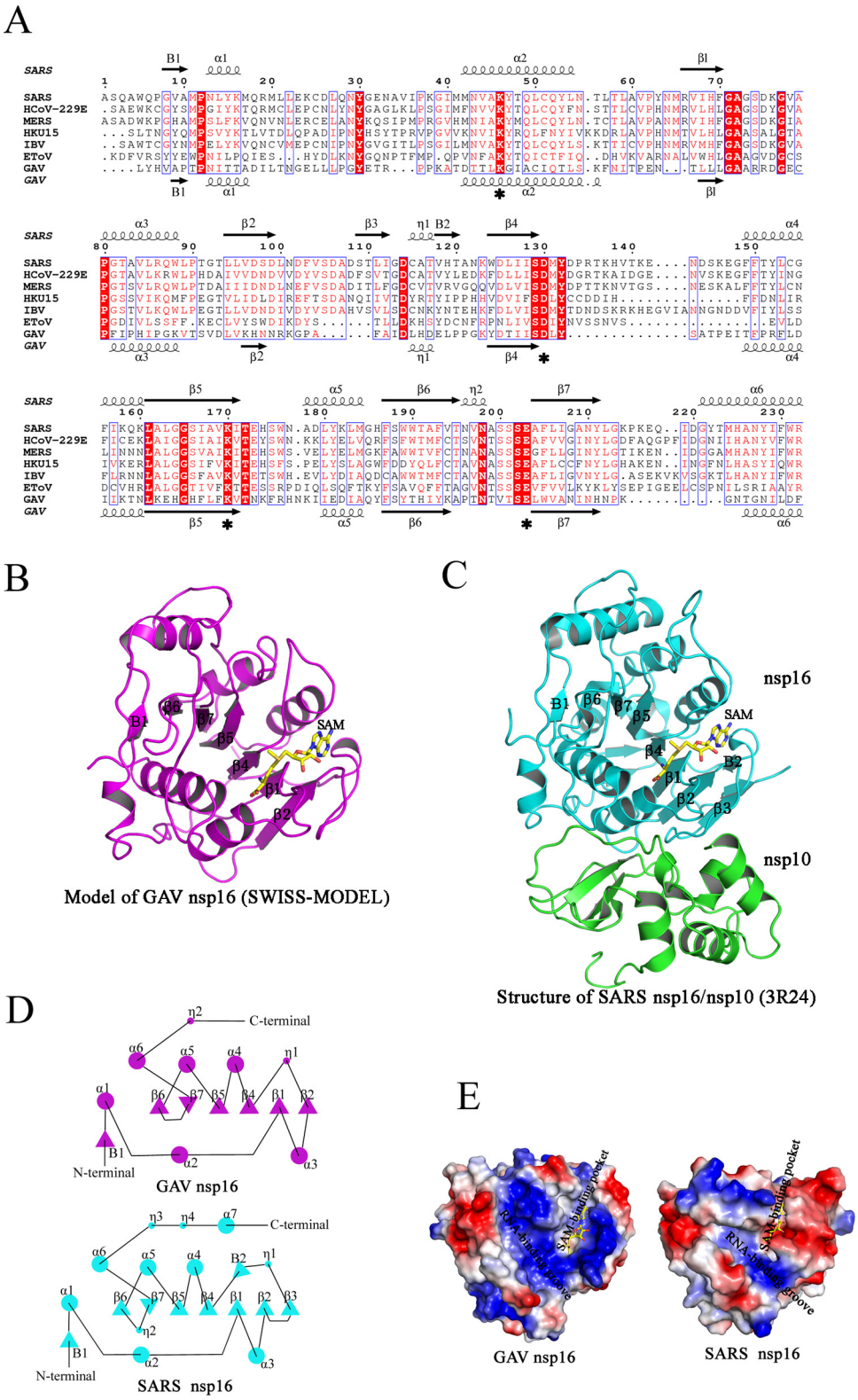

FIG 4 Sequence alignment and homology modeling of GAV nsp16. (A) Multiple-sequence alignment of selected 2′-*O*-methyltransferases of nidoviruses. The β-strands of the canonical MTase fold are labeled from β1 to β7, and additional β-strands from B1 onward. (B) Ribbon representation of the GAV nsp16 model structure, generated based on the template structure of SARS nsp10/nsp16 (PDB accession no. 3R24). (C) SAM was added to the GAV nsp16 model by superimposition of the model and the structure of SARS nsp10/nsp16 (PDB accession no. 3R24). The β-strands were marked in accordance with the alignment. (D) Schematic diagrams of the topologies of GAV nsp16 (modeled structure) and SARS nsp16. (E) Surface electrostatic potentials of GAV nsp16 (model) and SARS nsp16. The surface electrostatic potential diagram was generated by PyMol; the blue areas represent positively charged areas, while the red areas represent negatively charged areas.

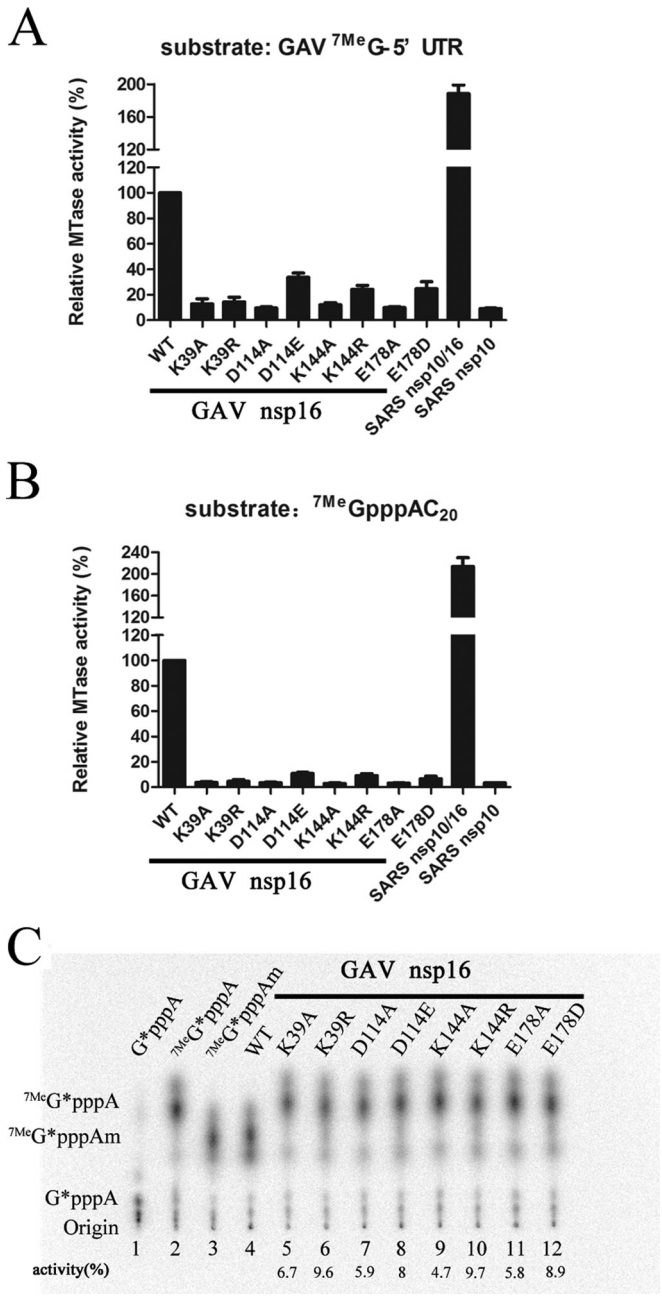

FIG 5 Activities of wild-type (WT) GAV nsp16 and K-D-K-E mutants. (A) MTase activities of GAV nsp16 (WT and mutants) detected by using ^{7Me}G-pppAC$_{20}$ as the substrate in ^{3}H-methyl incorporation assays. (B) MTase activities of GAV nsp16 (WT and mutants) detected by using ^{7Me}Gppp-RNA (GAV 5′ UTR) as the substrate in ^{3}H-methyl incorporation assays. (C) MTase activities of GAV nsp16 (WT and mutants) analyzed by RNA digestion and TLC assays. Lane 4 represents the WT of GAV nsp16; lane 2 is a negative control, lane 3 is a positive control treated with vaccinia virus VP39, and lanes 5 to 12 are mutants of GAV nsp16. The error bars indicate standard deviations.

(Fig. 5A) and the capped oligonucleotide ^{7Me}GpppAC$_{20}$ (Fig. 5B), were tested, and the results were consistent.

The 2′-*O*-MTase activities of GAV nsp16 mutants were also tested by nuclease P1 treatment and TLC assays. As shown in Fig. 5C, all the GAV nsp16 mutants were crippled in their 2′-*O*-MTase activities, which was in accordance with the results of the ^{3}H-methyl-labeled assays (Fig. 5A and B).

Taking the data together, we concluded that residues Lys-39, Asp-114, Lys-144, and Glu-178 of GAV nsp16 likely constitute the K-D-K-E catalytic tetrad that is essential for 2′-*O*-MTase activity.

Effects of MTase inhibitors on GAV nsp16 2′-*O*-MTase activity. To further characterize the enzymatic activity of GAV nsp16, we tested whether the activity could be inhibited by previously characterized MTase inhibitors, such as *S*-(5′-adenosyl)-L-homocysteine (SAH, or AdoHcy), sinefungin, and ribavirin. SAH is a by-product of the SAM-dependent methyl transfer reaction. Sinefungin is a SAM analog, and ribavirin is a GTP analog. These three small molecules have often been used to inhibit SAM-dependent methyltransferases (39, 44, 45). As shown in Fig. 6, sinefungin and AdoHcy were the most efficient inhibitors, and their half-maximal inhibitory concentrations (IC_{50}) were determined to be 28.7 and 73.9 μM, respectively (Fig. 6A and C). Ribavirin was much less efficient in our GAV nsp16 assay (Fig. 6B). Compared with the values reported for other viral 2′-*O*-MTases, we found that these three compounds had varying effects on different MTases. For examples, the IC_{50} of AdoHcy is 0.34 μM for the 2′-*O*-MTase of dengue virus NS5MTase$_{DV}$ (39) and 144 μM for FCoV nsp16 (20). Ribavirin did not exert a significant inhibitory effect on 2′-*O*-MTase of dengue virus NS5MTase$_{DV}$ (39), similar to our observations with GAV nsp16.

DISCUSSION

Nidoviruses have linear, single-stranded RNA genomes with positive polarity that contain a 5′ cap structure and a 3′ poly(A) tail (17). Several enzymes are involved in the formation of the 5′ cap structure of viral RNA and host mRNA, including RNA triphosphatase, guanylyltransferase, N7-MTase, and 2′-*O*-MTase (1, 2, 4). In coronaviruses, the N7- and 2′-*O*-MTases have been studied in the most detail, and the two enzymes were found to play important roles in the modification of the viral cap structure (5, 18, 22), while the RNA helicase nsp13 of coronaviruses could function as an RNA triphosphatase (46). Until now, the guanylyltransferase of coronaviruses has been completely unknown. However, no experimental evidence for the activities of these enzymes is available for any of the other nidoviruses, and in the case of arteriviruses, it has even become quite uncertain whether the viral replicase includes any MTases at all (47). Although bioinformatics analyses have predicted that roniviruses and toroviruses, like coronaviruses, encode a methyltransferase near the 3′ end of ORF1b (17, 34, 48), they were not confirmed experimentally. In this study, we expressed and purified the putative methyltransferases of EToV (torovirus) and GAV (ronivirus) according to the bioinformatics-based prediction of the natural replicase cleavage sites (30, 36), and we provided experimental evidence that GAV nsp16 indeed possesses 2′-*O*-MTase activity. Surprisingly, the torovirus nsp16, which is more closely related to coronavirus nsp16, did not show any 2′-*O*-MTase activity in our assays. The failure to detect 2′-*O*-MTase activity for torovirus nsp16 may reflect its intrinsic properties or the limitations of our assay. For example, torovirus nsp16 may require an additional protein cofactor other than the nsp10 used by coronaviruses or other RNA substrate requirements than those used here.

Our results indicate that, like the coronaviral 2′-*O*-MTase, GAV nsp16 can discriminate an N7-methylated RNA cap from a nonmethylated cap (20). This is different from other viral 2′-*O*-

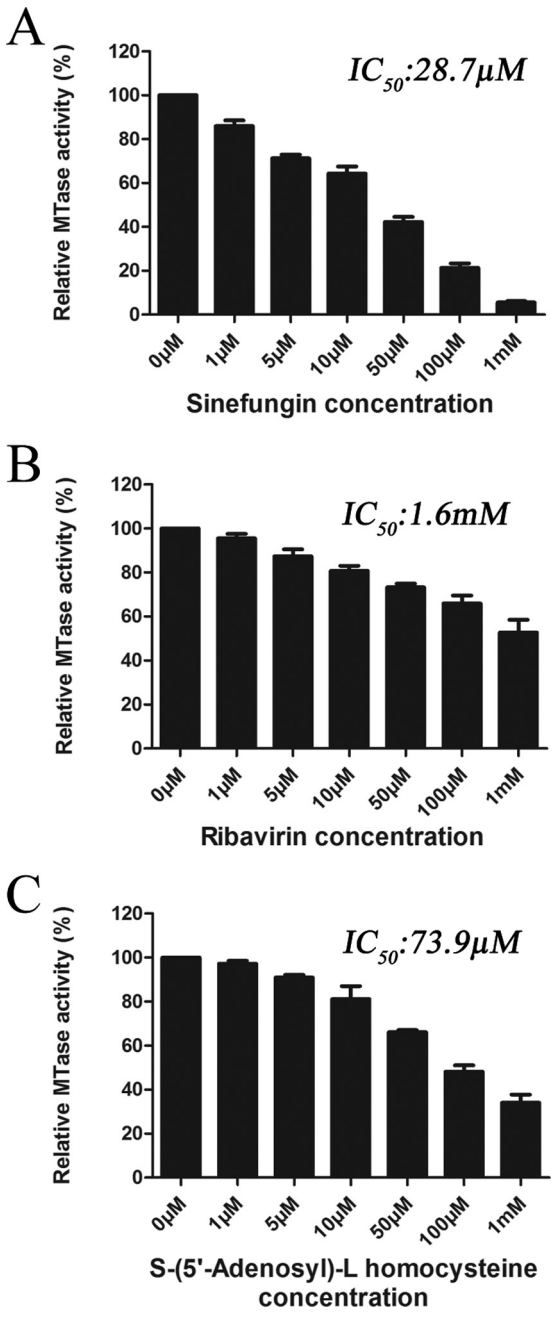

FIG 6 Inhibition of GAV nsp16 2′-*O*-MTase activity by established methyltransferase inhibitors. Increasing concentrations of sinefungin (A), ribavirin (B), and AdoHcy (a by-product of the reaction) (C) were added to the reaction mixtures, and the activity was measured by using ^{3}H-methyl incorporation MTase activity assays. The error bars indicate standard deviations.

MTases, such as those of dengue virus and Meaban virus, which are able to transfer methyl groups from AdoMet to both methylated and unmethylated RNA caps (GpppAC$_n$ and ^{7Me}GpppAC$_n$) at the 2′-O position of the first nucleotide (20, 39, 49, 50). GAV nsp16 can efficiently methylate only RNA substrates with a 5′-terminal A, similar to SARS-CoV nsp16, while vaccinia virus VP39 is a 2′-*O*-MTase that works in a sequence-nonspecific manner (37). This indicates that GAV nsp16 is a more specific cap-modifying enzyme in the recognition of 5′-capped viral RNA.

Interestingly, unlike coronavirus nsp16, *in vitro*, GAV nsp16 can function alone in the absence of any other viral protein, suggesting that *in vivo*, it also may not require a protein cofactor to stimulate its enzymatic activity. As shown in our previous work, SARS-CoV nsp10, the cofactor of the nsp16 2′-*O*-MTase, acts as a buttress to support the pocket involved in SAM binding and thus enhances the binding affinity for SAM (5).

The 3D structure model predicts that GAV nsp16 will have some remarkable difference from SARS-CoV nsp16. First, the SAM-binding pocket of GAV nsp16 appears to have a more rigid structure and may be stable enough to bind with the methyl donor SAM. In contrast, the SAM-binding pocket of SARS-CoV nsp16 possesses a flexible loop (residues 100 to 108) (Fig. 4). Second, the equivalent of the β3-strand of SARS-CoV nsp16 is predicted to be missing in GAV nsp16. Third, the analysis of the electrostatic potential shows that the RNA-binding groove on the surface of GAV nsp16 is longer than that of SARS nsp16 (Fig. 4E); the former is about 32 Å in length and fits well with the requirement for a 6-nt RNA substrate (^{7Me}GpppAC$_5$), which is consistent with our observation that the shortest RNA substrate on which GAV nsp16 showed 2′-*O*-MTase activity was 6 nt long (Fig. 2D). This observation may in part explain why GAV does not need a viral protein cofactor for its enzymatic activity, whereas SARS-CoV nsp16 requires nsp10 to extend its RNA-binding groove to accommodate its RNA substrate efficiently, as demonstrated in our previous study (5). These structural differences may contribute to the distinct properties of coronavirus and ronivirus 2′-*O*-MTases and thus may explain why ronivirus nsp16 does not need a protein cofactor for MTase activity.

Through sequence alignment and mutational analysis, we identified the conserved K-D-K-E catalytic tetrad of GAV nsp16, which is similar to that of the typical RNA cap-1 structure-modifying enzymes. The catalytic tetrad is K_{39}-D_{114}-K_{144}-E_{178} (Fig. 4A). Homology modeling showed that GAV nsp16 has a six-stranded β-sheet arrayed in parallel in the middle of the protein surrounded by α-helices and loops, while the β-sheet is seven stranded in SARS-CoV nsp16 and many other known 2′-*O*-methyltransferases (5, 43). Nevertheless, the six-stranded β-sheet is also reported for some other MTases, e.g., the RNA methyltransferase TlyA (51), which is missing the third β-strand located at the edge of the seven-stranded β-sheet structure. The four amino acid residues in the GAV nsp16 catalytic tetrad K_{39}-D_{114}-K_{144}-E_{178} of GAV nsp16 are located at positions similar to those of the tetrad K_{46}-D_{130}-K_{170}-E_{203} of SARS-CoV nsp16.

It is well-known that the cap structure is very important for mRNA stability and translation. It has been demonstrated that 2′-O methylation of viral RNA caps is also important for RNA viruses to evade host innate immune recognition (7, 8, 52). Therefore, viral capping enzymes are potential targets for antiviral drug development. Recently, we demonstrated that a coronavirus nsp10-derived short peptide can potently inhibit nsp16 2′-*O*-MTase activity *in vitro* and viral replication in animals (15). In the future, such small-molecule inhibitors can be developed to target the 2′-*O*-MTases of other nidoviruses that infect humans and mammals. In this study, we showed that the well-known MTase inhibitor sinefungin possesses inhibitory activity on GAV nsp16. Although it appears unlikely to produce efficient and cost-effective antiviral drugs against shrimp viruses, debilitation of GAV 2′-*O*-MTase may be used as a strategy to generate live attenuated

ronivirus vaccines, like that used to produce coronavirus and flavivirus vaccines (9–12).

In summary, we have identified and characterized the 2′-*O*-methyltransferase of GAV, extending our knowledge of RNA cap formation and methylation beyond coronaviruses in the order *Nidovirales*. The ronivirus 2′-*O*-MTase shows both similarities and unique features compared with the coronavirus 2′-*O*-MTase. The K-D-K-E catalytic tetrad of GAV nsp16 is well conserved, but ronivirus 2′-*O*-MTase does not require a protein cofactor to stimulate its activity and possibly possesses a six-stranded β-sheet instead of a canonical seven-stranded β-sheet in the core of the MTase structure.

ACKNOWLEDGMENTS

We thank J. A. Cowley for kindly providing GAV genome cDNA.

We thank Andong Wu (now in the Department of Health Technology Research and Development, Space Institute of Southern China, Shenzhen, Guangdong province, China) for his abundant exploratory work.

This study was supported by the China 973 Basic Research Program (2013CB911101) and China NSFC grants (81130083, 31170152, and 31000085) and by the Sigrid Juselius Foundation. D.G is also supported by the Hubei Provincial Medical Leading Expert Project.

FUNDING INFORMATION

This work, including the efforts of Deyin Guo, was funded by National Basic Research Program of China (973 Program) (2013CB911101). This work, including the efforts of Deyin Guo, was funded by Hubei Bureau of Science & Technology (2015CFA009). This work, including the efforts of Deyin Guo, was funded by Hubei Provincial Medical Leadership Project. This work, including the efforts of Yu Chen and Deyin Guo, was funded by National Natural Science Foundation of China (NSFC) (81130083 and 31000085). This work was funded by National Natural Science Foundation of China (NSFC) (31170152). This work, including the efforts of Tero Ahola and Deyin Guo., was funded by Sigrid Juséliuksen Säätiö (Sigrid Jusélius Stiftelse)

REFERENCES

1. **Ghosh A, Lima CD.** 2010. Enzymology of RNA cap synthesis. Wiley Interdiscip Rev RNA **1:**152–172. http://dx.doi.org/10.1002/wrna.19.
2. **Bouvet M, Ferron F, Imbert I, Gluais L, Selisko B, Coutard B, Canard B, Decroly E.** 2012. Capping strategies in RNA viruses. Med Sci (Paris) **28:**423–429. http://dx.doi.org/10.1051/medsci/2012284021.
3. **Furuichi Y, Shatkin AJ.** 2000. Viral and cellular mRNA capping: past and prospects. Adv Virus Res **55:**135–184. http://dx.doi.org/10.1016/S0065-3527(00)55003-9.
4. **Decroly E, Ferron F, Lescar J, Canard B.** 2012. Conventional and unconventional mechanisms for capping viral mRNA. Nat Rev Microbiol **10:**51–65. http://dx.doi.org/10.1038/nrmicro2675.
5. **Chen Y, Su C, Ke M, Jin X, Xu L, Zhang Z, Wu A, Sun Y, Yang Z, Tien P, Ahola T, Liang Y, Liu X, Guo D.** 2011. Biochemical and structural insights into the mechanisms of SARS coronavirus RNA ribose 2′-O-methylation by nsp16/nsp10 protein complex. PLoS Pathog **7:**e1002294. http://dx.doi.org/10.1371/journal.ppat.1002294.
6. **Chen Y, Guo D.** 2016. Molecular mechanisms of coronavirus RNA capping and methylation. Virol Sin **31:**3–11. http://dx.doi.org/10.1007/s12250-016-3726-4.
7. **Daffis S, Szretter KJ, Schriewer J, Li J, Youn S, Errett J, Lin TY, Schneller S, Zust R, Dong H, Thiel V, Sen GC, Fensterl V, Klimstra WB, Pierson TC, Buller RM, Gale M, Jr, Shi PY, Diamond MS.** 2010. 2′-O methylation of the viral mRNA cap evades host restriction by IFIT family members. Nature **468:**452–456. http://dx.doi.org/10.1038/nature09489.
8. **Zust R, Cervantes-Barragan L, Habjan M, Maier R, Neuman BW, Ziebuhr J, Szretter KJ, Baker SC, Barchet W, Diamond MS, Siddell SG, Ludewig B, Thiel V.** 2011. Ribose 2′-O-methylation provides a molecular signature for the distinction of self and non-self mRNA dependent on the RNA sensor Mda5. Nat Immunol **12:**137–143. http://dx.doi.org/10.1038/ni.1979.
9. **Zhang Y, Sun J, Wei Y, Li J.** 2016. A reverse genetics approach for the design of methyltransferase-defective live attenuated avian metapneumovirus vaccines. Methods Mol Biol **1404:**103–121. http://dx.doi.org/10.1007/978-1-4939-3389-1_7.
10. **Li SH, Dong H, Li XF, Xie X, Zhao H, Deng YQ, Wang XY, Ye Q, Zhu SY, Wang HJ, Zhang B, Leng QB, Zuest R, Qin ED, Qin CF, Shi PY.** 2013. Rational design of a flavivirus vaccine by abolishing viral RNA 2′-O methylation. J Virol **87:**5812–5819. http://dx.doi.org/10.1128/JVI.02806-12.
11. **Zust R, Dong H, Li XF, Chang DC, Zhang B, Balakrishnan T, Toh YX, Jiang T, Li SH, Deng YQ, Ellis BR, Ellis EM, Poidinger M, Zolezzi F, Qin CF, Shi PY, Fink K.** 2013. Rational design of a live attenuated dengue vaccine: 2′-O-methyltransferase mutants are highly attenuated and immunogenic in mice and macaques. PLoS Pathog **9:**e1003521. http://dx.doi.org/10.1371/journal.ppat.1003521.
12. **Menachery VD, Yount BL, Jr, Josset L, Gralinski LE, Scobey T, Agnihothram S, Katze MG, Baric RS.** 2014. Attenuation and restoration of severe acute respiratory syndrome coronavirus mutant lacking 2′-O-methyltransferase activity. J Virol **88:**4251–4264. http://dx.doi.org/10.1128/JVI.03571-13.
13. **Milani M, Mastrangelo E, Bollati M, Selisko B, Decroly E, Bouvet M, Canard B, Bolognesi M.** 2009. Flaviviral methyltransferase/RNA interaction: structural basis for enzyme inhibition. Antivir Res **83:**28–34. http://dx.doi.org/10.1016/j.antiviral.2009.03.001.
14. **Luzhkov VB, Selisko B, Nordqvist A, Peyrane F, Decroly E, Alvarez K, Karlen A, Canard B, Qvist J.** 2007. Virtual screening and bioassay study of novel inhibitors for dengue virus mRNA cap (nucleoside-2′O)-methyltransferase. Bioorg Med Chem **15:**7795–7802. http://dx.doi.org/10.1016/j.bmc.2007.08.049.
15. **Wang Y, Sun Y, Wu A, Xu S, Pan R, Zeng C, Jin X, Ge X, Shi Z, Ahola T, Chen Y, Guo D.** 2015. Coronavirus nsp10/nsp16 methyltransferase can be targeted by nsp10-derived peptide in vitro and in vivo to reduce replication and pathogenesis. J Virol **89:**8416–8427. http://dx.doi.org/10.1128/JVI.00948-15.
16. **Lauber C, Ziebuhr J, Junglen S, Drosten C, Zirkel F, Nga PT, Morita K, Snijder EJ, Gorbalenya AE.** 2012. Mesoniviridae: a proposed new family in the order Nidovirales formed by a single species of mosquito-borne viruses. Arch Virol **157:**1623–1628. http://dx.doi.org/10.1007/s00705-012-1295-x.
17. **Gorbalenya AE, Enjuanes L, Ziebuhr J, Snijder EJ.** 2006. Nidovirales: evolving the largest RNA virus genome. Virus Res **117:**17–37. http://dx.doi.org/10.1016/j.virusres.2006.01.017.
18. **Chen Y, Cai H, Pan J, Xiang N, Tien P, Ahola T, Guo D.** 2009. Functional screen reveals SARS coronavirus nonstructural protein nsp14 as a novel cap N7 methyltransferase. Proc Natl Acad Sci U S A **106:**3484–3489. http://dx.doi.org/10.1073/pnas.0808790106.
19. **Chen Y, Tao J, Sun Y, Wu A, Su C, Gao G, Cai H, Qiu S, Wu Y, Ahola T, Guo D.** 2013. Structure-function analysis of severe acute respiratory syndrome coronavirus RNA cap guanine-N7-methyltransferase. J Virol **87:**6296–6305. http://dx.doi.org/10.1128/JVI.00061-13.
20. **Decroly E, Imbert I, Coutard B, Bouvet M, Selisko B, Alvarez K, Gorbalenya AE, Snijder EJ, Canard B.** 2008. Coronavirus nonstructural protein 16 is a cap-0 binding enzyme possessing (nucleoside-2′O)-methyltransferase activity. J Virol **82:**8071–8084. http://dx.doi.org/10.1128/JVI.00407-08.
21. **Bouvet M, Debarnot C, Imbert I, Selisko B, Snijder EJ, Canard B, Decroly E.** 2010. In vitro reconstitution of SARS-coronavirus mRNA cap methylation. PLoS Pathog **6:**e1000863. http://dx.doi.org/10.1371/journal.ppat.1000863.
22. **Decroly E, Debarnot C, Ferron F, Bouvet M, Coutard B, Imbert I, Gluais L, Papageorgiou N, Sharff A, Bricogne G, Ortiz-Lombardia M, Lescar J, Canard B.** 2011. Crystal structure and functional analysis of the SARS-coronavirus RNA cap 2′-O-methyltransferase nsp10/nsp16 complex. PLoS Pathog **7:**e1002059. http://dx.doi.org/10.1371/journal.ppat.1002059.
23. **Cowley JA, Dimmock CM, Spann KM, Walker PJ.** 2001. Gill-associated virus of Penaeus monodon prawns. Molecular evidence for the first invertebrate nidovirus. Adv Exp Med Biol **494:**43–48.
24. **Cowley JA, Walker PJ.** 2002. The complete genome sequence of gill-associated virus of Penaeus monodon prawns indicates a gene organisation unique among nidoviruses. Arch Virol **147:**1977–1987. http://dx.doi.org/10.1007/s00705-002-0847-x.
25. **Wijegoonawardane PK, Cowley JA, Phan T, Hodgson RA, Nielsen L,**

Kiatpathomchai W, Walker PJ. 2008. Genetic diversity in the yellow head nidovirus complex. Virology **380:**213–225. http://dx.doi.org/10.1016/j.virol.2008.07.005.

26. **Cowley JA, Cadogan LC, Wongteerasupaya C, Hodgson RA, Boonsaeng V, Walker PJ.** 2004. Multiplex RT-nested PCR differentiation of gill-associated virus (Australia) from yellow head virus (Thailand) of Penaeus monodon. J Virol Methods **117:**49–59. http://dx.doi.org/10.1016/j.jviromet.2003.11.018.
27. **Cowley JA, Dimmock CM, Wongteerasupaya C, Boonsaeng V, Panyim S, Walker PJ.** 1999. Yellow head virus from Thailand and gill-associated virus from Australia are closely related but distinct prawn viruses. Dis Aquat Organ **36:**153–157. http://dx.doi.org/10.3354/dao036153.
28. **Wijegoonawardane PK, Sittidilokratna N, Petchampai N, Cowley JA, Gudkovs N, Walker PJ.** 2009. Homologous genetic recombination in the yellow head complex of nidoviruses infecting Penaeus monodon shrimp. Virology **390:**79–88. http://dx.doi.org/10.1016/j.virol.2009.04.015.
29. **Cowley JA, Dimmock CM, Spann KM, Walker PJ.** 2000. Gill-associated virus of Penaeus monodon prawns: an invertebrate virus with ORF1a and ORF1b genes related to arteri- and coronaviruses. J Gen Virol **81:**1473–1484. http://dx.doi.org/10.1099/0022-1317-81-6-1473.
30. **Ziebuhr J, Bayer S, Cowley JA, Gorbalenya AE.** 2003. The 3C-like proteinase of an invertebrate nidovirus links coronavirus and potyvirus homologs. J Virol **77:**1415–1426. http://dx.doi.org/10.1128/JVI.77.2.1415-1426.2003.
31. **Sittidilokratna N, Dangtip S, Cowley JA, Walker PJ.** 2008. RNA transcription analysis and completion of the genome sequence of yellow head nidovirus. Virus Res **136:**157–165. http://dx.doi.org/10.1016/j.virusres.2008.05.008.
32. **Nga PT, Parquet MDC, Lauber C, Parida M, Nabeshima T, Yu F, Thuy NT, Inoue S, Ito T, Okamoto K, Ichinose A, Snijder EJ, Morita K, Gorbalenya AE.** 2011. Discovery of the first insect nidovirus, a missing evolutionary link in the emergence of the largest RNA virus genomes. PLoS Pathog **7:**e1002215. http://dx.doi.org/10.1371/journal.ppat.1002215.
33. **Zirkel F, Kurth A, Quan PL, Briese T, Ellerbrok H, Pauli G, Leendertz FH, Lipkin WI, Ziebuhr J, Drosten C, Junglen S.** 2011. An insect nidovirus emerging from a primary tropical rainforest. mBio **2:**e00077–00011. http://dx.doi.org/10.1128/mBio.00077-11.
34. **Snijder EJ, Bredenbeek PJ, Dobbe JC, Thiel V, Ziebuhr J, Poon LL, Guan Y, Rozanov M, Spaan WJ, Gorbalenya AE.** 2003. Unique and conserved features of genome and proteome of SARS-coronavirus, an early split-off from the coronavirus group 2 lineage. J Mol Biol **331:**991–1004. http://dx.doi.org/10.1016/S0022-2836(03)00865-9.
35. **Ahola T, Laakkonen P, Vihinen H, Kaariainen L.** 1997. Critical residues of Semliki Forest virus RNA capping enzyme involved in methyltransferase and guanylyltransferase-like activities. J Virol **71:**392–397.
36. **Smits SL, Snijder EJ, de Groot RJ.** 2006. Characterization of a torovirus main proteinase. J Virol **80:**4157–4167. http://dx.doi.org/10.1128/JVI.80.8.4157-4167.2006.
37. **Hodel AE, Gershon PD, Quiocho FA.** 1998. Structural basis for sequence-nonspecific recognition of 5′-capped mRNA by a cap-modifying enzyme. Mol Cell **1:**443–447. http://dx.doi.org/10.1016/S1097-2765(00)80044-1.
38. **Jeffery DR, Roth JA.** 1987. Kinetic reaction mechanism for magnesium binding to membrane-bound and soluble catechol O-methyltransferase. Biochemistry **26:**2955–2958. http://dx.doi.org/10.1021/bi00384a042.
39. **Selisko B, Peyrane FF, Canard B, Alvarez K, Decroly E.** 2010. Biochemical characterization of the (nucleoside-2′O)-methyltransferase activity of dengue virus protein NS5 using purified capped RNA oligonucleotides (7Me)GpppAC(n) and GpppAC(n). J Gen Virol **91:**112–121. http://dx.doi.org/10.1099/vir.0.015511-0.
40. **Barbosa E, Moss B.** 1978. mRNA(nucleoside-2′-)-methyltransferase from vaccinia virus. Characteristics and substrate specificity. J Biol Chem **253:**7698–7702.
41. **Egloff MP, Benarroch D, Selisko B, Romette JL, Canard B.** 2002. An RNA cap (nucleoside-2′-O-)-methyltransferase in the flavivirus RNA polymerase NS5: crystal structure and functional characterization. EMBO J **21:**2757–2768. http://dx.doi.org/10.1093/emboj/21.11.2757.
42. **Feder M, Pas J, Wyrwicz LS, Bujnicki JM.** 2003. Molecular phylogenetics of the RrmJ/fibrillarin superfamily of ribose 2′-O-methyltransferases. Gene **302:**129–138. http://dx.doi.org/10.1016/S0378-1119(02)01097-1.
43. **Martin JL, McMillan FM.** 2002. SAM (dependent) I AM: the S-adenosylmethionine-dependent methyltransferase fold. Curr Opin Struct Biol **12:**783–793. http://dx.doi.org/10.1016/S0959-440X(02)00391-3.
44. **Pugh CS, Borchardt RT, Stone HO.** 1978. Sinefungin, a potent inhibitor of virion mRNA(guanine-7-)-methyltransferase, mRNA(nucleoside-2′-)-methyltransferase, and viral multiplication. J Biol Chem **253:**4075–4077.
45. **Pugh CS, Borchardt RT.** 1982. Effects of S-adenosylhomocysteine analogues on vaccinia viral messenger ribonucleic acid synthesis and methylation. Biochemistry **21:**1535–1541. http://dx.doi.org/10.1021/bi00536a011.
46. **Ivanov KA, Thiel V, Dobbe JC, van der Meer Y, Snijder EJ, Ziebuhr J.** 2004. Multiple enzymatic activities associated with severe acute respiratory syndrome coronavirus helicase. J Virol **78:**5619–5632. http://dx.doi.org/10.1128/JVI.78.11.5619-5632.2004.
47. **Lehmann KC, Hooghiemstra L, Gulyaeva A, Samborskiy DV, Zevenhoven-Dobbe JC, Snijder EJ, Gorbalenya AE, Posthuma CC.** 2015. Arterivirus nsp12 versus the coronavirus nsp16 2′-O-methyltransferase: comparison of the C-terminal cleavage products of two nidovirus pp1ab polyproteins. J Gen Virol **96:**2643–2655. http://dx.doi.org/10.1099/vir.0.000209.
48. **von Grotthuss M, Wyrwicz LS, Rychlewski L.** 2003. mRNA cap-1 methyltransferase in the SARS genome. Cell **113:**701–702. http://dx.doi.org/10.1016/S0092-8674(03)00424-0.
49. **Peyrane F, Selisko B, Decroly E, Vasseur JJ, Benarroch D, Canard B, Alvarez K.** 2007. High-yield production of short GpppA- and 7MeGpppA-capped RNAs and HPLC-monitoring of methyltransfer reactions at the guanine-N7 and adenosine-2′O positions. Nucleic Acids Res **35:**e26. http://dx.doi.org/10.1093/nar/gkl1119.
50. **Mastrangelo E, Bollati M, Milani M, Selisko B, Peyrane F, Canard B, Grard G, de Lamballerie X, Bolognesi M.** 2007. Structural bases for substrate recognition and activity in Meaban virus nucleoside-2′-O-methyltransferase. Protein Sci **16:**1133–1145. http://dx.doi.org/10.1110/ps.072758107.
51. **Arenas NE, Salazar LM, Soto CY, Vizcaino C, Patarroyo ME, Patarroyo MA, Gomez A.** 2011. Molecular modeling and in silico characterization of Mycobacterium tuberculosis TlyA: possible misannotation of this tubercle bacilli-hemolysin. BMC Struct Biol **11:**16. http://dx.doi.org/10.1186/1472-6807-11-16.
52. **Garcia-Sastre A.** 2011. 2 Methylate or not 2 methylate: viral evasion of the type I interferon response. Nat Immunol **12:**114–115. http://dx.doi.org/10.1038/ni0211-114.